# A High-Order Method for Wave Propagation in 3D Dielectric Waveguides of Arbitrary Transverse Shape

Final Report

John Emmons, Emmanuel Garza, and Oscar Bruno

*California Institute of Technology, Applied and Computational Mathematics*
*1200 East California Boulevard, Pasadena, CA 91125*

**Abstract**

Dielectric waveguides play essential roles in fiber optic devices, wireless communication, and other specialized electronics. However, modeling the propagation of electromagnetic fields in dielectric waveguides of arbitrary shapes presents several challenges. In particular, the mode spectrum consists of a discrete and continuous set of eigenfunctions and the continuous modes require special treatment to avoid low order convergence. Previous works do not fully address these challenges or ignore them altogether, limiting their use to simplified cases and making them unsuitable for physically realistic simulations.

We present progress on a general, high-order numerical method for simulating dielectric waveguides with complex 3D geometries, requiring only modest computational resources (a single workstation). The method is based on first expanding fields into the modes of the waveguide, then propagating the expansion to simulate the field. We characterize the continuous spectrum of radiation modes and make progress toward a general prescription for its discretization. Using this approach, we can compute a highly accurate expansion of an arbitrary field into the modes of the waveguide, including discrete and continuous modes, yielding a more general technique for high precision dielectric waveguide simulations.

## 1. Introduction

Metallic and dielectric waveguides direct electromagnetic waves to travel along their optical axis. The propagation of electromagnetic waves inside a waveguide is often described using a geometric optics approximation in which only the center of energy of the wave is tracked. However, waveguides with diameters near the wavelength of a propagating field cannot be accurately described by this approximate geometric model; rather, simulations of the propagation of the field must be done by solving Maxwell's equations inside (and outside in the case of dielectric media) the waveguide.

In most cases, it is impossible to find closed-form solutions for waveguides with complex boundaries. Hence, numerical methods must be used to approximate the solutions of these problems. Developing accurate, high-order numerical methods for simulating the propagation of electromagnetic fields inside and outside of a dielectric waveguide is essential for continued advancement in the design of specialized devices such as dielectric antennas with complicated geometries.

Previous work in this area has focused only on circular waveguides (8), where solutions have a closed form expression. Even for the circular case, it is typical to do certain approximations (e.g. assuming that there is a small difference in premittivity between the core and cladding for dielectric waveguides, which leads to ignoring the reflected field at interfaces). For the case of 2D waveguides, a more complete set of theory and methods exists since there are analytical expressions for the modes of planar waveguides (6), but the generalization to three dimensions is not trivial. Modes for 3D waveguides depend on the geometry and there only exist closed form expressions for symmetric shapes.

Even more recent efforts still focus on radially symmetric waveguides (7). On the other hand, little attention has been given to arbitrary shaped 3D waveguides beyond computing the field as an expansion of bound modes (4); as a result, radiation away from the core of the waveguide cannot be modeled. Other methods that take into account the fields away from the core usually suffer from different limitations. For example, some methods introduce an artificial boundary in order to truncate the domain (2) which leads to unphysical reflections that do not correspond to the behavior of the fields. In this project, we sought to solve all these problems by developing, implementing, and benchmarking a method that is high-order for arbitrary 3D geometries.

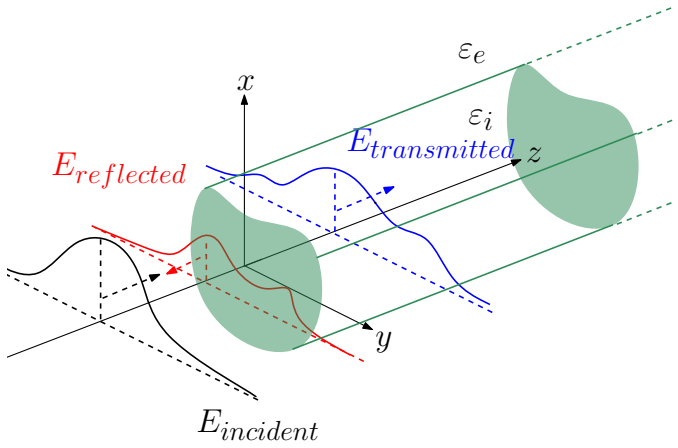


Figure 1: This diagram gives a graphical depiction of the illumination problem. For a known incident field that illuminates the waveguide, we seek to find the reflected and transmitted fields by computing the expansion of these fields into the modes of the waveguide. To do this, we must first numerically find the modes, then use high-order methods to compute the projection of the field onto each mode, yielding the expansion. Once the expansion is found, we can easily simulate the propagation of the field.

## 2. Objective

The goal of this project was to develop and characterize a robust and high-order numerical method to analyze the excitation of optical modes (bounded and continuous) in a 3D dielectric waveguide with an arbitrary incident field. We used a physically realistic model which unlike previous works (2; 4; 7), does not introduce approximations to the domain or limit use to symmetric systems. This method expands the field into eigenmodes of the waveguide (discrete and continuous spectrum), then propagates the expansion to yield an accurate simulation method (overall goal illustrated in figure 1).

There were several challenges encountered because of this approach. Firstly, due to the open nature of dielectric waveguides, the complete set of eigenmodes includes a continuous spectrum that makes the mode decomposition a mix of an integral with unknown amplitude function, in addition to the traditional sum of modes with unknown amplitude coefficients. There is no general approach used to discretize the continuous spectrum for arbitrary geometries. Developing a method to properly discretize these modes was a key component of this work and is an area that still requires additional research.

Another challenge in the simulation of such problems is the treatment of the discontinuous permittivity along the boundary of the waveguide. Computing projections onto the modes requires 2D integrals over these discontinuous regions; the spatial order of accuracy would be limited to first order (even for high-order methods) if no special consideration for these discontinuities was made. Developing a general, high-order 2D integration method to address this challenge was vital to the success of the project. Solving these two challenges were the goals set by mentor (Emmanuel Garza) and PI (Oscar Bruno) at the beginning of the summer.

## 3. Summary of Work Completed

The following sections contain a description of the theory, methods, and results of the numerical method developed over the course of the summer. Work related to the project but not necessary a component of the method is also included since much of the summer was spent on these related topics.

### *3.1. Theoretical Background*

Maxwell's equations are the classical model for describing electromagnetic interactions. In a dielectric material,

$$\nabla \cdot \mathbf{D} = \rho_f \tag{1.1}$$

$$\nabla \cdot \mathbf{B} = 0 \tag{1.2}$$

$$\nabla \times \mathbf{E} = -\frac{\partial \mathbf{B}}{\partial t} \tag{1.3}$$

$$\nabla \times \mathbf{H} = \mathbf{J}_f + \frac{\partial \mathbf{D}}{\partial t} \tag{1.4}$$

$\mathbf{E}$, $\mathbf{B}$, $\mathbf{J}_f$, and $\rho_f$ are the electric field, magnetic field, current density, and charge density respectively. $\mathbf{D}$ and $\mathbf{H}$ are defined as:

$$\mathbf{D} \equiv \varepsilon \mathbf{E} \tag{2.1}$$

$$\mathbf{H} \equiv \frac{1}{\mu} \mathbf{B} \tag{2.2}$$

When Maxwell's equations are analyzed near the boundary between two dielectrics (as in fig. 2 at the interface between $\varepsilon_i$ and $\varepsilon_\ell$), they impose a set

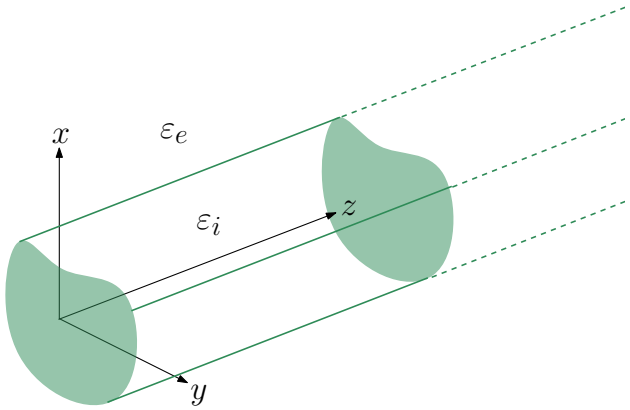


Figure 2: Cross section of a non-uniformly shaped waveguide extending from 0 to $+\infty$ along the z-axis. Note the different permittivities in the core of the waveguide ($\varepsilon_i$) and in the cladding ($\varepsilon_e$).

of boundary conditions which must be satisfied along the boundary of the waveguide (figure 2):

$$\varepsilon_1 E_1^{\perp} - \varepsilon_2 E_2^{\perp} = 0 \tag{3.1}$$

$$\mathbf{H}_1 - \mathbf{H}_2 = 0 \tag{3.2}$$

$$E_1^{\parallel} - E_2^{\parallel} = 0 \tag{3.3}$$

Furthermore, by taking a time harmonic field, and assuming that the solutions only depend on $z$ by a factor of $e^{ik_z z}$ (where $k_z$ is the unknown longitudinal wavenumber), we have that Maxwell's equations simplify to solving a set of coupled Helmoltz equations in two different regions:

$$\left.\begin{aligned} \nabla_t^2 H_z + \gamma_1^2 H_z &= 0 \\ \nabla_t^2 E_z + \gamma_1^2 E_z &= 0 \end{aligned}\right\} \text{in } \Omega_1 \tag{4.1}$$

$$\left.\begin{aligned} \nabla_t^2 H_z + \gamma_2^2 H_z &= 0 \\ \nabla_t^2 E_z + \gamma_2^2 E_z &= 0 \end{aligned}\right\} \text{in } \Omega_2 \tag{4.2}$$

with the corresponding boundary conditions:

$$E_{z,1} = E_{z,2} \tag{5.1}$$

$$H_{z,1} = H_{z,2} \tag{5.2}$$

$$\frac{\varepsilon_1}{\gamma_1^2}\frac{\partial E_{z,1}}{\partial n} - \frac{\varepsilon_2}{\gamma_2^2}\frac{\partial E_{z,2}}{\partial n} = -\frac{\omega\mu_0}{k_z}\left(\frac{\varepsilon_1}{\gamma_1^2} - \frac{\varepsilon_2}{\gamma_2^2}\right)\frac{\partial H_z}{\partial T}\bigg|_{\partial\Omega} \tag{5.3}$$

$$\frac{1}{\gamma_1^2}\frac{\partial H_{z,1}}{\partial n} - \frac{1}{\gamma_2^2}\frac{\partial H_{z,2}}{\partial n} = -\frac{\omega}{k_z}\left(\frac{\varepsilon_2}{\gamma_2^2} - \frac{\varepsilon_1}{\gamma_1^2}\right)\frac{\partial E_z}{\partial T}\bigg|_{\partial\Omega} \tag{5.4}$$

where $\Omega_1$ is the domain corresponding to the core (the $\varepsilon_i$ region in fig. 2), $\Omega_2$ refers to the domain of the cladding (the $\varepsilon_e$ region in fig. 2) and $\gamma_1^2 = \varepsilon_1\mu_0\omega^2 - k_z^2$ and $\gamma_2^2 = \varepsilon_2\mu_0\omega^2 - k_z^2$ are the transverse wavenumbers. Note that in this notation $\hat{n}$ is the normal vector that points outwards, i.e. away from the interior of $\Omega_1$, while we have $\hat{T} = \hat{z} \times \hat{n}$ is the tangential vector that is directed in a counterclockwise sense (1).

Due to the symmetry of the waveguide, once we know the longitudinal components of the fields, we can compute the other four transverse components by:

$$\mathbf{E}_t = \begin{cases} \frac{i}{\gamma_1^2}\left(k_z\nabla_t E_z - \omega\mu_0\hat{z}\times\nabla_t H_z\right), \text{ in } \Omega_1 \\ \frac{i}{\gamma_2^2}\left(k_z\nabla_t E_z - \omega\mu_0\hat{z}\times\nabla_t H_z\right), \text{ in } \Omega_2 \end{cases} \tag{6.1}$$

$$\mathbf{H}_t = \begin{cases} \frac{i}{\gamma_1^2}\left(k_z\nabla_t H_z + \omega\varepsilon_1\hat{z}\times\nabla_t E_z\right), \text{ on } \Omega_1 \\ \frac{i}{\gamma_2^2}\left(k_z\nabla_t H_z + \omega\varepsilon_2\hat{z}\times\nabla_t E_z\right), \text{ on } \Omega_2 \end{cases} \tag{6.2}$$

The solutions to these equation are called the modes of the waveguide. Modes fall into two categories: bounded and continuous (sometimes called radiative). The bounded modes are confined to travel inside the waveguide; in fiber optic communication, these modes are the most important since they will propagate for long distances with low attenuation. However, in this project we also interested in the continuous modes, which unlike bounded modes, extend to infinity outside of the waveguide and interact with surrounding materials.

Because of the linearity of Maxwell's Equations, the total electric and magnetic fields for a waveguide is the superposition of bounded and continuous modes. Furthermore, it can be shown that bounded modes form a discrete

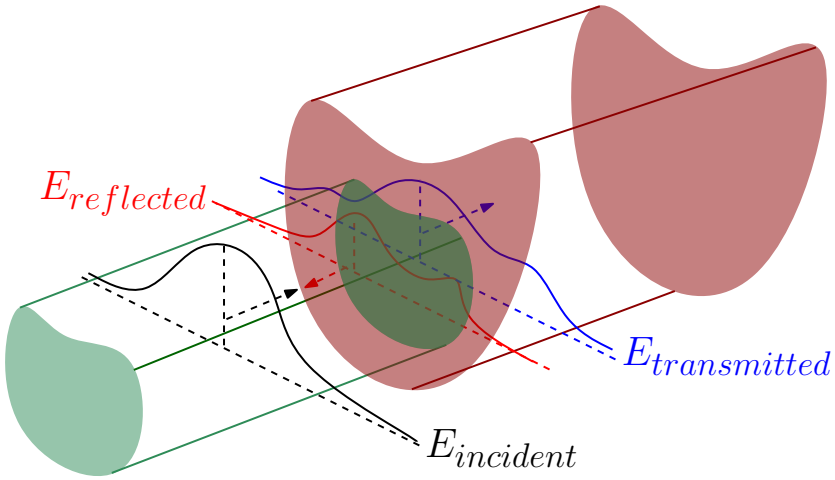


Figure 3: In our method, we want to simluate the reflected and transmitted fields that are generated at the interface of two waveguides with different geometries. We planned to do this by implementing a mode matching scheme in 3D, something that had never been done before in these types of problems. This feature was not successfully implemented because of time constraints, but is still an active area of research.

spectrum while the continuous modes form a continuous spectrum.

$$\mathbf{E}_{total} = \sum_i a_i \, \mathbf{E}^i_{bound} + \mathbf{E}_{rad} \tag{7.1}$$

$$\mathbf{B}_{total} = \sum_i a_i \, \mathbf{B}^i_{bound} + \mathbf{B}_{rad} \tag{7.2}$$

Since the bounded modes are discrete (in fact finite for dielectric waveguides), their contribution to the total field can be written as a sum as seen above. On the other hand, there are uncountably many continuous modes so they cannot be summed in the same way; to find their contribution to the total field, we must now take an integral over all the continuous modes.

$$a_i = \frac{1}{2N_i} \int_{A_\infty} \mathbf{E}_t \times \mathbf{h}^*_{ti} \cdot \hat{\mathbf{z}} \, dA \tag{8.1}$$

$$\mathbf{E}_{rad} = \sum_i \int_0^\infty a_i(Q) \, \mathbf{e}_i \, e^{i\beta(Q)z} \, dQ \tag{8.2}$$

$$\mathbf{H}_{rad} = \sum_i \int_0^\infty a_i(Q) \, \mathbf{h}_i \, e^{i\beta(Q)z} \, dQ \tag{8.3}$$

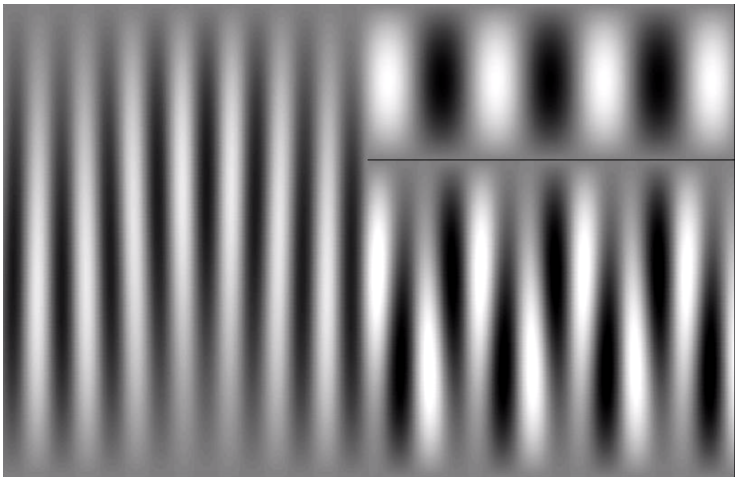

Figure 4: The image shows the simulation a wave traveling in a 2D perfect electrical conductor (PEC) waveguide which splits into two smaller waveguides (division marked with black horizontal line). Mode matching is used to compute the transmitted and reflected fields in all thee regions. In mode matching, a system of equations is constructed using the boundary conditions of the waveguide and the given incident field, then the system is solved to find the coefficients for the modes (forward and backward propagating).

Once we have solved for the coefficients of the bounded and continuous mode for a given incident field, we will have solved the problem of illumination.

*3.2. Mode Matching for PEC in 2D*

The long-term goal of this project was to accurately simulate the propagation of an arbitrary field including what happens at the boundary of two 3D dielectric waveguides with differing geometries (as illustrated in figure 3). This goal required many other parts of the method to be implemented first, but to gather a general understanding of the approach I started the summer by implementing a simplified version in 2D.

I began by writing a code to take an arbitrary field in a perfect electrical conductor (PEC) planar waveguide and propagate its expansion past a discontinuity. In this particular problem, the waveguide (width $a$) was split into two smaller waveguides (width $b$ and $c$ such that $a = b + c$) by a perfect barrier. In order to do this, I first solved (analytically) for the modes of a rectangular PEC waveguide. The solution for this was already known and can be readily found in many introductory electromagnetic theory text books. However, deriving the expressions starting with only Maxwell's Equations was a good exercise for reviewing the basics.

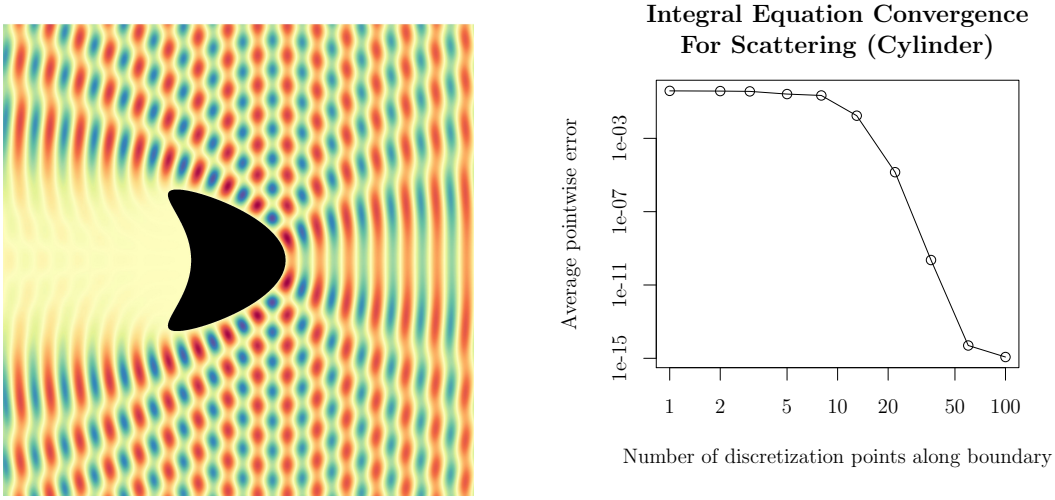


Figure 5: [left] The scattering problem is solved with an integral equation approach for a 2D PEC kite with an incoming plane wave from the $+x$-axis. The values of the density along the boundary of the kite are found by solving a system of equations created with the governing PDEs and incoming field. Once the electron density is found, computing the field is easy given basic equations from electrostatic. The magnitude of the field is plotted in the figure. [right] The convergence of integral equation methods is spectral in the case of scattering problems. To show this, we compute the exact value of the field when solving the scattering problem for a cylinder (for which an analytical solution exists) and compare it to the results obtained by the numerical results using integral equations. The convergence is shown to the spectral by the exponential decay in the error of the field.

Once I had derived the expressions for the modes, I implemented a simple code to propagate and visualize the fields. The final step was to solve for the mode coefficients in the waveguides of width $b$ and $c$ given the coefficients in the waveguide of width $a$. This was done by constructing a systems of equations from the boundary conditions and given incident field, then solving this system. The results this work can be seen in figure 4. The first mode of the waveguide is incident on the barrier, producing a reflected and transmitted field in the waveguide.

### *3.3. Integral Equation Methods for 2D Scattering*

Our wavguide simulation method relies on integral equations to numerically find the modes for arbitrary geometries with high-order convergence. In order to become more familiar with the approach, I implemented a scattering problem solver with integral equations. This would be useful later since

computing the modes numerically requires solving a scattering problem in a dielectric.

An integral equation is an equation where the function of interest appears under an integral sign.

$$f(x) = \int K(x,t)\,\varphi(t)\,dt. \tag{9}$$

Equation 9 is an integral equation if $f(x)$ and $\varphi(t)$ and known and the function of interest is $K(x,t)$ is unknown. To solve these problems numerically, we discretize the variable $x$, then solve the linear system of equations that is created by approximating the integral.

These methods have many advantages over simpler methods. For example, finite difference methods must spatially discretize a domain; this is nontrivial for problems where the domain is infinite. In the case of scattering, the fields extend to infinity everywhere, so special consideration would have to be taken to solve these problems with a finite difference solver. With integral equations though, we do not discretize the domain spatially; rather, we discretize along the boundary of the scattering object. No special consideration is required to account for truncatation or fields which do not decay rapidly.

For scattering by a PEC object, the unknown function is the electron density along the boundary. It is easy to compute the field everywhere once the density on the boundary is known ($\boldsymbol{E} = \frac{1}{4\pi\varepsilon_0}\int \frac{\hat{\boldsymbol{r}}}{r^2}\rho\,d\tau$), so the goal was to write a code to find the electron density using integral equations. Figure 5 (on the left), shows the results of this work for a kite shaped boundary, which demonstrates that is approach works for arbitrary geometries. The field is plotted around the object in black with an incident field incoming from the $+x$ axis.

On the right of figure 5, the convergence of the integral equation methods is shown for the scattering problem for a cylinder (for which the analytical solution is easy to compute). Note that the error between the numerical and analytical solution decreases super-algebraically as the number of mesh points along the boundary increases. This is expected because it is possible to prove integral equation methods converence super-algebraically (3).

### *3.4. Projections for 3D Dielectric Waveguide of Arbitrary Shape*

The solutions to Maxwell's equations in a 3D dielectric waveguide has a high degree of degeneracy. In fact, there are uncountably many modes for all 3D dielectric waveguides (solutions to Maxwell's equations of the form

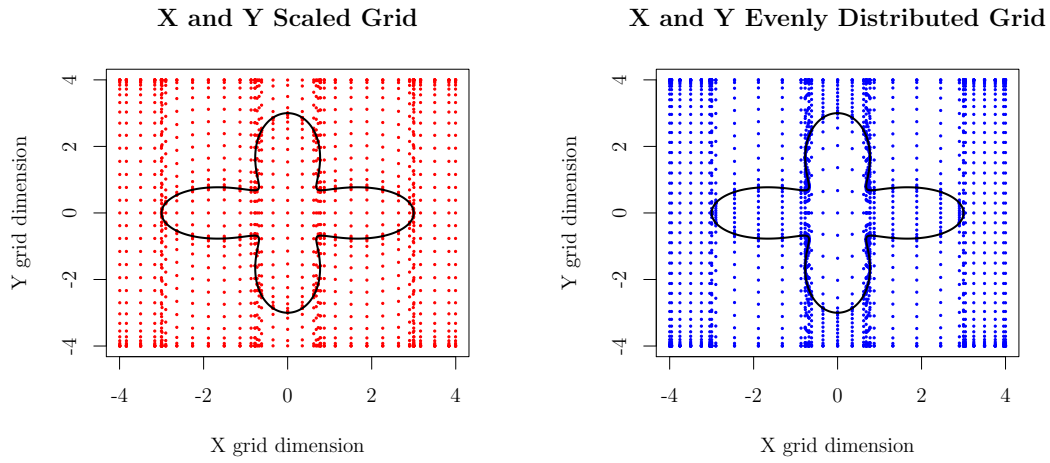


Figure 6: These meshes are generated by the adaptive grid implementation using different strategies to assign points to subintervals. Each mesh uses the same number of points, but arranges them differently. [Left] In the scaled strategy, points are assigned evenly along each dimension. In this way, intervals receive a number of mesh points proportional to their length (like the House of Representatives in Congress). [Right] In the even strategy, points are split evenly among intervals without regard for their relative length (like the Senate in Congress). When tested, the even distribution strategy produces the highest order of convergence.

$\boldsymbol{E}(x, y)\, e^{ik_x z}$). We seek to compute the expansion of an arbitrary field into these modes of the waveguide so we can simulate the propagation of the field with high-order convergence and for general geometries. Computing the expansion is analogous to finding the Fourier transform for a function. In the same way, we can recover the original field by multiplying the modes by their corresponding coefficients and summing/integrating.

$$\mathbf{E}_{total} = \sum_{i=1}^{N} a_i\, \mathbf{E}^i_{bound} + \sum_j \int_0^\infty a_j(Q)\, \mathbf{e}_j\, e^{i\beta(Q)z}\, dQ \tag{10a}$$

where

$$a_i = \frac{1}{2N_i} \int_{A_\infty} \mathbf{E}_t \times \mathbf{h}^*_{ti} \cdot \hat{\mathbf{z}}\, dA \tag{10b}$$

Note that $\mathbf{E}_{total}$ (the total electric field) is composed of a discrete (the sum) and a continuous (the integral) spectrum of modes; the same is true of the magnetic field $\mathbf{H}_{total}$. Choosing an appropriate discretization of the continuous modes was one of the primary research questions I tried to answer this summer.

In order to compute the projection of an arbitrary field onto the modes of the waveguide (i.e. the coefficient in equation 10b), we need to be able to compute 2-dimensional integrals with high-order convergence. This is a not a trivial task in this case because the field is discontinuous at the boundary of the interior and exterior of the waveguide and the fields can in general decay slowly away from the waveguide. As a result, we cannot use simple methods (such as trapezoidal integration) to preform these integrals because they are low-order when there are discontinuities in the function.

To address this issue, I helped design and implement a generic 2D integration method which is high-order regardless of the shape of the waveguide boundary. The idea is to divide the domain of integration in such as way as to avoid integrating over any discontinuities, then use high-order quadrature rules for each smaller intervals.

To divide the region, the method first identifies locations along the curve where the x derivative of the parameterization is zero (i.e where the curve goes straight up or down in figure 6). These points represents locations along the x-dimension where the function could have a discontinuous jump. The method then discretize these intervals using a high-order method, Colton & Kress (3), to obtain the location of the columns (i.e. x grid). The next step is to identify locations where the columns intersect the curve and create grids in a similar way as before in the y dimension (creating the y grid). Combining these two, we have a non-uniform grid in x and y which avoids discontinuities. This adaptive grid is able to achieve high-order accuracy even for functions with $C^1$ discontinuities.

However, even after completing the implementation described above, the method was not able to achieve the high-order accuracy that we expected. In figure 7, both curves use exactly the same method to compute the intervals over which the integrals are taken; however, the order of accuracy is very different. The difference in figure 7 can be attributed to the way we assign discretization points to the intervals in the domain. There are two strategies for assigning points that we tried: scaling the number of points based on interval length and dividing points evenly among intervals without considering length. In figure 6, the curve labeled with evenly distributed shows the

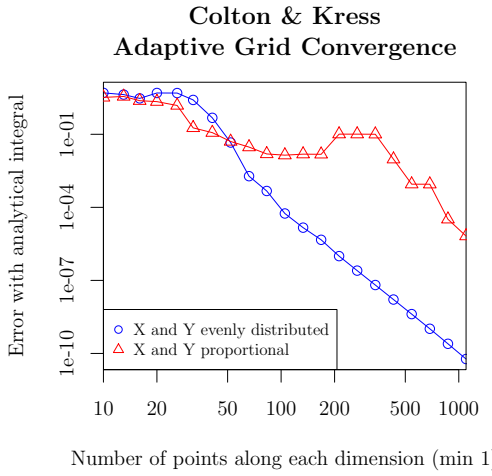


Figure 7: The convergence of the adaptive grid method is implemented using different stratgies to assign points to the integration intervals. The blue curve with circles shows the convergence when the points are assigned evenly to each interval of integration without scaling by the length. Surprisingly, the convergence for this method is better than when the number of points is proportional on the interval length (as seen by the red curve with triangles). This result can be explained by the upper bound on the error for the quadrature rule, given by $|E^{(n)}(f)| \leq \frac{C}{n^{2q+1}}$. In second strategy, few points are given to smaller intervals when the mesh density is increased. As a result, larger intervals which are already well resolved continue to receive more points while small intervals with large errors continue to have large errors. Eventually this causes small intervals to limit the accuracy.

convergence when points are assigned to integration intervals without regard to interval length. For example, if the user wants 100 points in the x dimension and the code divides the region into 4 intervals, then each interval gets 25 points (even if some of the intervals are much smaller than others). This can be seen by the variation in the spacing of grid points in figure 6.

Using the evenly divided strategies surprisingly gives the best convergence results. We are able to justify this result, but it was not obvious. Our reasoning is the error in the scaled spacing method is bounded below by the interval with the lowest points per unit length. If short intervals are assigned points according to there length, then large parts of the integral may not be resolved well since larger intervals are the first to receive new points. By evenly distributing points, we ensure the error is bounded above by the largest intervals, which receive points at the same rate at small intervals; ensuring convergence.

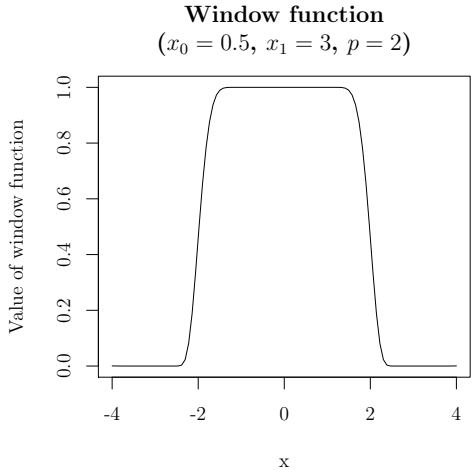


Figure 8: When the Bruno-Monro window function is applied to integrands which oscillate and decay slowly, the convergence of numerical integration methods can be greatly improved (spectral convergence can be obtained in some cases). We use the window function when computing the expansion of the incident field into the continuous modes (continuous modes oscillate a decay slowly away from the waveguide, perfect for use with the window function).

*Convergence of Expansion Coefficients for Continuous Modes*

Once the adaptive grid implementation was completed and fully debugged for the bounded modes (which decay exponentially fast away from the waveguide), the next step was to test the convergence of the method for a continuous mode. In general, the continuous modes oscillate and decay slowly (proportional to $\frac{1}{\sqrt{r}}$), making the convergence of naïve integration methods slow. Previous work done in this area by Oscar Bruno, et. al. confirms that using simple integration methods such as trapezoidal integration are low-order when the function oscillates and decays slowly (e.g. $\mathbb{R}^2$ in our case). The low-order of convergence is the result of truncating the domain and making the following approximation

$$\int_0^\infty \frac{e^{ir}}{\sqrt{r}} dr \approx \int_0^A \frac{e^{ir}}{\sqrt{r}} dr \quad \text{(for large A, but converges slowly)}$$

The solution is to apply the Bruno-Monro windowing function to the integrand (window function illustrated in figure 8). A discussion of this function is beyond the scope of this report, but by modifying the integrand,

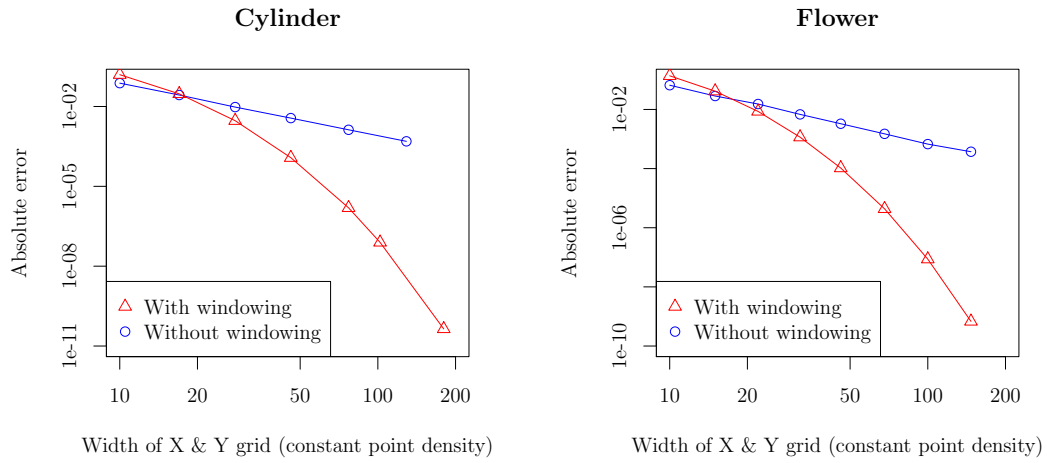


Figure 9: We integrate a modified Hankel function ($\frac{1}{z^2}H_0^1(z)$) on $\mathbb{R}^2$ outside of a cylindrical and flower shaped waveguide (the continuous modes will be a supposition of Hankel function for the cylinder, so testing this function is a useful measure of success for our method). [Left] For the cylindrical waveguide, the Hankel function is centered at the origin. The error of integration is found by comparing the numerical result to the analytical solution. [Right] For the flower waveguide, the Hankel function is centered at $(0.5, 0.5)$ (a point still inside the waveguide but no longer symmetric). The error is computed by comparing the numerical result to a value obtained by using same method with a much larger window size (assumed to be converged). In both cases, as the truncated domain of integration is increased, the convergence is exponential with the windowing function and is approximately second order without the windowing function.

super-algebraic convergence can be achieved; see (5) for more details. Figure 9 compares the windowing function approach to simple truncation. With the addition of the windowing function, the integration method developed in previous section is able to integrate both bounded and continuous modes with high-order convergence and is ready to be used for computing eigenfunction expansion coefficients.

*Convergence of Modal Eigenvalues*

After completing the integration method for computing the expansion coefficients, it was now possible to propagate an arbitrary field along the waveguide with high accuracy. However, before additional work could be done, it was important to comfirm the expected order of convergence is acheived with all the parts in place. Debugging at this stage was especially

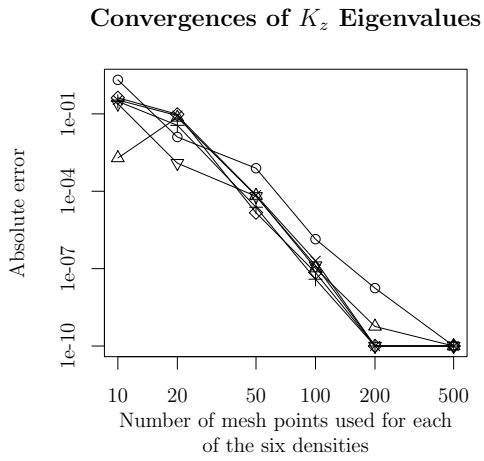


Figure 10: The convergence of the discrete mode eigenvalues for the flower are shown as the the number of points used to discretize the six single layer densities along boundaries of the waveguide is increased. This illustrates that the methods used to compute these eigenvalues has high-order convergence and is suitable for our waveguide simulation method.

important because the problems we are solving are sufficiently complicated that we cannot confirm with analytical results. One check I performed was to ensure that the computed eigenvalues for the discrete and continuous spectrum converged appropriately.

In figure 10, the convergence plots of the six discrete eigenvalues for the flower geometry are shown. We used a reliable benchmark as the accepted value to compute the error. As expected, the convergence is very high-order (approximately sixth order) and is same for all eigenvalues.

*Orthogonality of Discrete and Continuous Modes*

As part of confirming the correctness of the code, we also performed tests to ensure the discrete and continuous modes we computed numerical were orthogonal, meaning the inner product of any mode (discrete or continuous) with any other mode was zero. The property of orthogonality is vital when computing projections. In the case of discrete modes, we saw that the spectrum was indeed orthogonal up to the accuracy of the methods used.

$$\int_{\mathbb{R}^2} E^{\mu}_{\text{inc}} \times \bar{H}^{\lambda}_{\text{mode}} dA = \delta(\mu - \lambda) \tag{11}$$

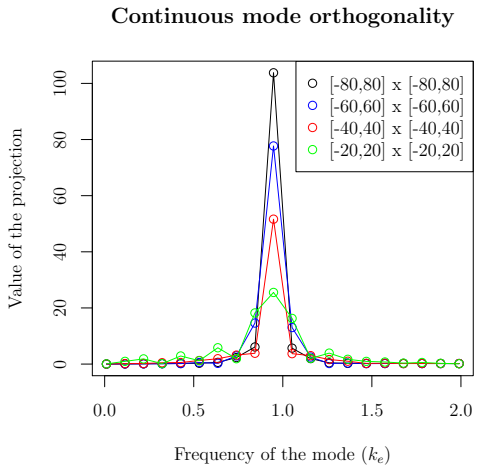


Figure 11: A continuous mode with frequency ($k_e$) of 0.9479 is projected onto other continuous modes to test orthogonality. The different lines show the orthogonality obtained for different sized domains of integration. As the domains tend to infinity, the curves approach a Dirac delta function demonstrating that as our discretization grows larger we approach the expected analytical result.

In the case of continuous modes, confirming orthogonality was less trivial; specifically, the continuous modes are not integrable. In the analytical case, we expect the inner product of a continuous modes with other continuous modes to be a Dirac delta function (as seen in equation 11) centered at the frequency of the mode. Since we discretized (and truncated) the spatial dimension used to compute inner products, it was impossible to get the analytical result numerically. However, we can still confirm orthogonality by examining the limiting behavior of the inner product. Figure 11, illustrates the orthogonality of the modes as the mesh used to compute the inner product tends to $\mathbb{R}^2$. As expected, the curve approaches the delta function in equation 11.

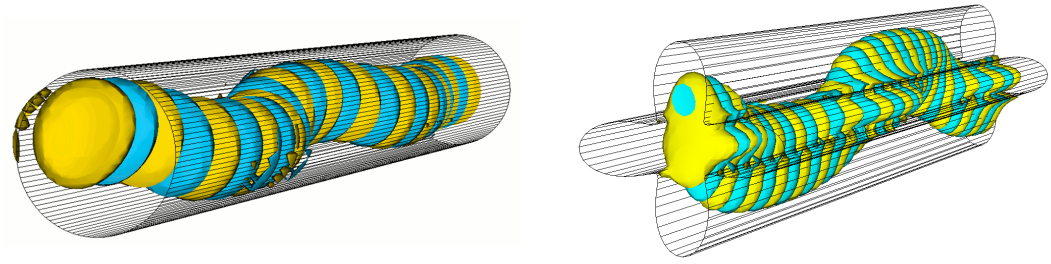

Figure 12: [left] A field with an intensity proportional to a Gaussian is applied to a cylindrical dielectric waveguide. The Gaussian field is not centered on the waveguide's optical axis; thus making the field oscillate as it propagates. For the cyliner, the modes can be compute analytically and these analytical modes are used to expand the incident field and simluate its propagation. No convergence study was performed, but the fields appear physically correct and confirm that our method was implemented without major errors. [right] The same Gaussian field applied to a flower shaped waveguide and using the numerically compute modes, the field is propagated. Once again, the field appears physically correct and confirms that the method is properly implemtened.

*Results*

During the summer, I completed the following tasks:

- Refreshed basic electromagnetic theory & partial differential equations
- Learned the integral equation numerical method
- Learned other relevant theoretical concepts (e.g. mode matching, high-order quadrature methods)
- Implemented a mode expansion method for 2D and 3D PEC waveguide
- Implemented a mode matching solver in 2D
- Solved the scattering problem using integral equations in 2D
- Implemented high-order 2D integration method for general waveguide shapes
- Implemented a mode expansion method for 3D dielectric waveguides

After doing all of these things, I was then able to obtain a few interesting results before the end of the internship. The goal of my project was to propagate an arbitrary field along a dielectric waveguide with arbitrary shape using a mode expansion method. As can be seen in figure 12, I was able

to complete this goal (note: I only show the cylinder and flower, but the algorithm is general and can produce these results for any shape).

Figure 12 shows the result of applying a non-centered Gaussian field at the end of a waveguide. The field is decomposed into the bounded modes of the waveguide, then the bound modes are individually propagated along the waveguide and summed to figure 12. Note, we do not include the continuous modes in this simulation because I was unable to fully debug the continuous spectrum before leaving for the summer; this is an area for future work. The analytical result exists for the cylinder in the left of figure 12, so it is possible to benchmark the rate of convergence; however, since we are only using bound modes such a convergence study is not useful since the error is bounded by the portion of the field projected into continuous modes. Once the implementation is completed and includes the continuous modes, a convergence study will be performed.

The partial results obtained with just the bound modes is promising nonetheless. In both the left and right of 12, the field are physically correct up to the correct error order (additional confirmation is still required) and the propagation appears to match my group's intuition about the solutions to such problem.

*Future Work*

The first thing that must be completed to continue work on this problem is to finish the implementation of the continuous modes. This will make the method fully capable of expanding and propagating any field along any dielectric waveguide. However, even after the continuous mode code is completed, there are a few expected challenges that will have to be solved.

Firstly, the discretization of the continuous spectrum must be solved more rigorously. To reiterate, the continuous modes form a spectrum with constants of propagation that extend from 0 to infinity. Figure 13 plots the projections of a Gaussian field onto the modes of a cylindrical waveguide. It is not obvious how we would integrate underneath that curve without encountering discontinuous jumps and other phenomena that make even sophisticated quadrature rules converge with low-order.

Secondly, once the mode expansion method is completed, the next step will be to include this method as part of a more general waveguide simulation tool. The goal is to develop a method that can accurately simulate the propagation of electromagnetic waves in general geometries, not just perfectly straight waveguides. An integral equation method to solve for the field in

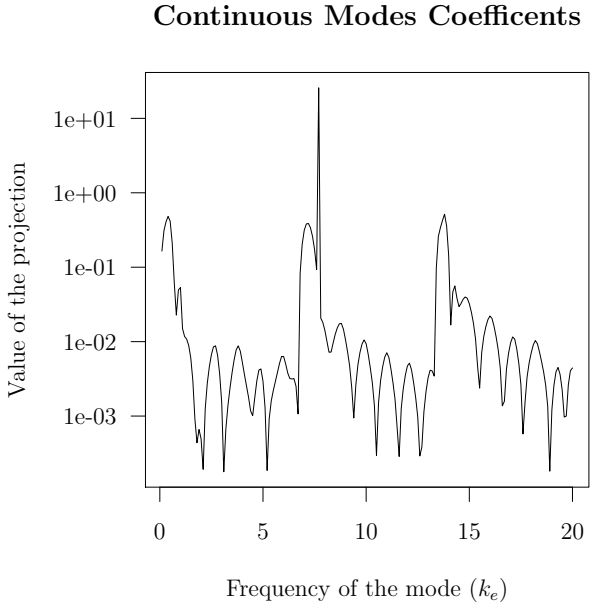


Figure 13: For the cylindrical wavguide, the continous modes can be found analytically; we found these analytical modes and used them to expand a Gaussian field (same as in figure 12) and plot the amplitude of the projections as a function of the propagation constant $k_e$. The cefficient vary wildly and approach zero discontinuously several times making the discretization of $k_e$ not trivial. Finding a method to discretize the continuous spectrum for a high-order method is an area of future work.

non-waveguide regions (i.e. dielectrics with highly irregular shapes) has already been proposed, but not implemented for the 3D case. Once this solver is implemented, it can be combined with the work I did this summer to produce a method that can solve waveguide problems with high-order for very general geometries.

## 4. Acknowledgments

I would like to thank the SFP office at Caltech for supporting my work by providing a summer research fellowship. I am also very thankful for the guidance my PI, Oscar Bruno, provided throughout my entire project. Finally, my graduate student mentor, Emmanuel Garza, deserves special thanks for the help he provided me on a daily basis; I would not have been able to accomplish nearly as much without his assistance.

## References


[1] J. D. L. Allan W. Snyder. Optical Waveguide Theory. Springer, 1 edition, 2003.

[2] G. Ciraolo and R. Magnanini. Analytical results for 2-d non-rectilinear waveguides based on the green's function. Mathematical Methods in the Applied Sciences, pages 1–18, 2007.

[3] D. Colton. Inverse acoustic and electromagnetic scattering theory, second edition, 1998.

[4] W. Lu and Y. Y. Lu. Waveguide mode solver based on Neumann-to-Dirichlet operators and boundary integral equations. Journal of Computational Physics, 231:1360–1371, 2012.

[5] J. A. Monro and O. P. Bruno. A super-algebraically convergent, windowing-based approach to the evaluation of scattering from periodic rough surfaces, 2007.

[6] F. S. Rolnado Magnanini. Wave propagation in a 2-d optical waveguide. SIAM Applied Mathematics, 2000.

[7] F. Santosa and R. Magnanini. Wave Propagation in a 3D Optical Waveguide. SIAM Journal on Applied Mathematics, 61(1):1237–1252, 2001.

[8] A. W. Snyder and D. J. Kinsley. Transactions on Microwave Theory and Techniques. IEEE, pages 1138–1144, 1969.